Periodically Poled Lithium Niobate Waveguides for Quantum Frequency Conversion

J. E. Toney*, V. E. Stenger, A. Pollick, J. Retz, P. Pontius, S. Sriram
SRICO, Inc.
2724 Sawbury Boulevard, Columbus, OH 43235, jtoney@srico.com

Abstract: This paper presents techniques for modeling annealed proton exchange (APE) and reverse proton exchange (RPE) waveguides in periodically poled lithium niobate for application to optical frequency conversion. A combination of time-dependent diffusion modeling and electromagnetic mode analysis using the RF module are used to predict the relationship between the poling period and the second harmonic generation (SHG) spectrum. Experimental SHG data are used to adjust the model, and calculated periodic poling periods are compared with measured results. Multi-mode effects are incorporated into the model and compared with experimental trends. The resulting model is successful in predicting the poling period for a given SHG process within 0.5 μm over the fundamental wavelength range from 1.5 to 2.0 μm.

Keywords: Nonlinear Optics, Optical Waveguides, Diffusion, PPLN

1. Introduction

Optical frequency conversion based on nonlinear optical interactions in periodically poled lithium niobate (PPLN) is finding widespread application in the burgeoning field of quantum information processing. Second harmonic generation in PPLN can be used to convert between the 700 - 800 nm wavelength band where single-photon emitters and detectors are most effective and the 1550 nm band for minimum transmission loss over optical fiber [1]. Spontaneous parametric down-conversion (SPDC) in PPLN can be used to generate polarization-entangled photon pairs for quantum key distribution and other applications [2].

To determine the proper poling period for a given frequency conversion process, the dispersion of the waveguide must be known accurately. This presents a particular challenge in lithium niobate, since waveguides are fabricated by diffusion, and the effective indices of the waveguide depend sensitively on the details of the dopant distribution.

COMSOL Multiphysics can be used to simulate the diffusion processes in detail, avoiding the need for simplifying assumptions. The primary challenge is determining the model parameters – temperature-dependent diffusion coefficients, initial concentration, and relationship between dopant concentration and refractive index.

2. Second-Order Nonlinear Optical Processes [3]

Second-order nonlinear optical (NLO) interactions are sometimes referred to as "three-wave mixing," since they involve interactions among three optical waves of wavelengths λ_1, λ_2 and λ_3. To conserve energy, these three wavelengths must satisfy the relation (by convention taking λ_1 to be the shortest wavelength):

$$\frac{1}{\lambda_1} = \frac{1}{\lambda_2} + \frac{1}{\lambda_3} \tag{1}$$

The second requirement for a three-wave interaction is momentum conservation, i.e. *phase matching*. In the *absence* of a periodic structure, the requirement (in one spatial dimension) is:

$$\frac{n_1}{\lambda_1} = \frac{n_2}{\lambda_2} + \frac{n_3}{\lambda_2} \tag{2}$$

where n_1, n_2 and n_3 are the refractive indices at the respective wavelengths. In a bulk device, the birefringence of the crystal is often utilized to satisfy equation (2) by proper selection of the propagation direction(s) relative to the crystal axes. That is not generally an option in a waveguide device, so instead the technique of *quasi-phase matching* (QPM) is used.

In QPM, the optic axis of the crystal is periodically reversed by application of a high voltage to create oppositely oriented ferroelectric domains. This process, *periodic poling*, creates a

structure in which the sign of the nonlinear optical coefficient reverses periodically. The momentum conservation condition is then modified as:

$$\frac{n_1}{\lambda_1} - \frac{n_2}{\lambda_2} - \frac{n_3}{\lambda_3} = \frac{1}{\Pi} \qquad (3)$$

where Π is the period, or pitch, of the structure.

If two of the wavelengths are specified, the third is determined by equation (1). The necessary poling period to realize that frequency conversion process is then determined by equation (3). Note that accurate determination of Π requires accurate knowledge of the dispersion relation of the material. For bulk devices the indices can be determined from published temperature- and wavelength-dependent Sellmeier equations, but in waveguide devices the effective indices must be determined through detailed modeling.

2.1 PPLN Waveguides

In bulk NLO devices the efficiency is limited by divergence of the beam, with most of the conversion occurring near the beam waist, where the intensity is highest. Optical waveguides are used to maintain high incremental conversion efficiency throughout the length of the device.

In $LiNbO_3$ most waveguides are fabricated by diffusion of dopants – either titanium ions or protons in most cases – to a depth of a few microns. The refractive index increases with dopant concentration, so that the diffused region forms the waveguide core.

Proton-exchanged waveguides are preferred for high-power applications, since they are less susceptible to "optical damage" from photorefractive effects. However, this class of waveguides only guides e-waves (polarized parallel to the optics axis). If both e- and o-waves must be supported, Ti-diffused waveguides are used. This paper focuses exclusively on proton-exchanged waveguides.

In proton exchange, protons are substituted for lithium ions in the $LiNbO_3$ lattice. After the initial proton exchange step (in-diffusion of protons to a depth of 1-2 microns by immersing the crystal in benzoic acid or other proton source) an annealing step at 300 – 350 ^oC is carried out to diffuse the protons and restore the NLO coefficient in the near-surface region. The result is an *annealed proton exchange (APE)* waveguide.

APE waveguides have an asymmetric mode profile and relatively high dispersion, since the peak index occurs at the $LiNbO_3$-air interface. A more symmetrical, buried index profile can be achieved by an additional step called *reverse proton exchange (RPE).* In RPE, the APE waveguide is immersed in a lithium-rich salt solution, allowing lithium ions to displace some of the previously introduced protons near the surface. The result is an index profile that peaks at a depth of 2-3 microns beneath the surface, producing a more symmetrical mode profile with less dispersion, better overlap among the shorter- and longer-wavelength waves, and higher input/output coupling efficiency to single-mode optical fiber.

2.2 Types of 3-Wave Interactions

There are several types of 3-wave interactions, classified as follows:

i. Second harmonic generation (SHG) : Input wave at $\lambda_2 = \lambda_3$, output wave at $\lambda_1 = \lambda_2/2$
ii. Sum Frequency Generation (SFG): Input waves at λ_2 and λ_3, output wave at λ_1
iii. Spontaneous Parametric Down-Conversion (SPDC): Input wave at λ_1, output waves at λ_2 and λ_3
iv. Difference Frequency Generation (DFG): Input waves at λ_1 and λ_2, output wave at λ_3. Note that for energy to be conserved in this case there must be two output photons at λ_2 for each input photon at λ_2. For this reason DFG is sometimes called optical parametric amplification (OPA).

Figure 1 illustrates each of these processes.

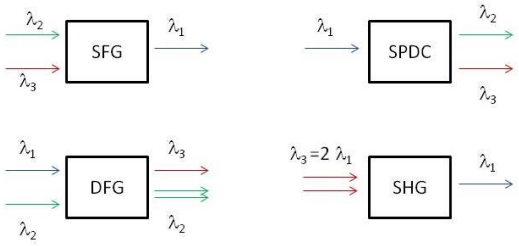

Figure 1. Illustration of second-order (i.e. 3-wave mixing) nonlinear processes.

2.3 Conversion Efficiency

Equation (3) gives the condition under which a particular frequency conversion process can occur in a periodically poled structure, but it says nothing about the efficiency of that process. The conversion efficiency is determined by the overlap among the modes by

$$\eta = \eta_0 \left| \int_{-\infty}^{\infty} dx \int_{-\infty}^{\infty} dy \ \hat{E}_1(x,y)\hat{E}_2(x,y)\hat{E}_3^*(x.y) \right|^2$$

$$\eta_0 = \frac{8\pi^2 d_{eff}^2}{n_1 n_2 n_3 c \epsilon_0 \lambda_3^2} \qquad (4)$$

where d_{eff} is the effective nonlinear optical coefficient for the interaction, c is the speed of light and ε_0 is the permittivity of free space. $_{1,}$ $_{2}$ $_{3}$ are the normalized mode fields at λ_1, λ_2 and λ_3, respectively, and E^* is the complex conjugate of E.

η_0 has dimensions of one-over-power, and the square of the overlap integral is one over the effective area, so that η is efficiency per unit input power, per length-squared. The output power after propagating a distance L is then

$$P_3(L) = \eta P_1(0) P_2(0) L^2 \qquad (5)$$

with $P_1(0)$ and $P_2(0)$ being the power of the two input waves at the input of the PPLN structure. This relation is typically expressed as slope efficiency in %/W:

$$\frac{P_3(L)}{P_1(0)P_2(0)} x100\% = \eta L^2 \qquad (6)$$

For SHG, this can be written as

$$\frac{P_3(L)}{P_1(0)^2} x100\% = \frac{\eta}{4} L^2 \qquad (7)$$

The factor-of-four reduction is usually explained s bei g ue to " ege er c y f c tor " but it c be viewed more simply by thinking of the input wave as two waves, each containing half the power.

2.4 Coupling Efficiency

Equation (6) gives the *internal* coupling efficiency – $P_1(0)$, $P_2(0)$, and $P_3(L)$ are the power levels of the waves entering and exiting the PPLN structure itself, without accounting for coupling loss between the $LiNbO_3$ chip and input/output fibers. The coupling efficiency can be calculated from an overlap integral between the fiber mode and the waveguide mode(s) at the input wavelength(s). The fiber mode can be taken as a Gaussian, so that the coupling efficiency as a function of vertical offset, y_0, can be calculated as:

$$\eta_{coup} = \frac{\left| \int_{-\infty}^{\infty} dx \int_{-\infty}^{\infty} dy \ \hat{E}_1(x,y) e^{-(y-y_0)^2/\sigma^2} \right|^2}{\left| \int_{-\infty}^{\infty} dx \int_{-\infty}^{\infty} dy \ e^{-(y-y_0)^2/\sigma^2} \right|^2} \qquad (8)$$

3. Model Construction

COMSOL Multiphysics 4.2 was used to construct a model of APE and RPE waveguides. The output of the model was imported to Scilab for calculation of the QPM period and conversion efficiency. The COMSOL model contained four study steps, the first three being time-dependent diffusion models using the Transport of Dilute Species interface, and the last being an optical mode calculation using the RF Module.

1. *Diffusion model to simulate the proton exchange step*. A fixed-concentration boundary condition was applied at the surface of the $LiNbO_3$ wafer over a width equal to the lithographically defined waveguide width. The boundary concentration, C_0, was adjusted to fit experimental SHG data (see Section 4). It is the only adjustable parameter in the model.

   The effective diffusion coefficient (which represents a combined diffusion of protons into the surface and lithium ions out) was calculated from a published temperature-dependent equation of the form [4]

   $$D_e(T) = D_{0e} e^{-Q/RT} \qquad (9)$$

   Q is the activation energy, T is the temperature in Kelvin, and R is the universal gas constant.

2. *Diffusion model to simulate the post-proton exchange annealing step*. The concentration profile from the proton exchange step was used as the initial condition for a second

diffusion step that simulated the annealing process.

The diffusion coefficient for protons in $LiNbO_3$ was calculated based on a published temperature-dependent equation of the form [5]:

$$D(T) = D_0 e^{-T_0/T} \qquad (10)$$

Equation (10) is comparable to equation (9) but expressed in slightly different form, following the practice of the authors of the respective references. A two-hour linear ramp-up and ramp-down of the temperature was incorporated via a user-defined function.

3. *Diffusion model to simulate the reverse proton exchange step*. The concentration profile output by step 2 was taken as the initial condition for step 3. The diffusion coefficient in $LiNbO_3$ was calculated from (10). In the region above the $LiNbO_3$ surface, corresponding to the salt solution, the diffusion coefficient was set several orders of magnitude higher, so that the salt bath acted as essentially a perfect sink for protons. As with step 2, a two-hour linear ramp-up and ramp-down of the temperature was incorporated via a user-defined function.

4. *Optical mode calculation at all wavelengths for the NLO interaction being studied*. The substrate index was calculated from the published Sellmeier relations, and the refractive index change was taken as proportional to the dopant distribution from the output of step 3. (See Section 4.1.)

Table 1 gives the model parameters, and Figure 2 show the impurity distribution after proton exchange, after annealing, and after reverse proton exchange. Figure 3 shows the calculated optical modes at wavelengths of 986 and 1972 nm, which are the wavelengths for an experimental SHG case study presented in Section 4.3 below.

Additional parameters that enter into the model are the temperatures and times for the proton exchange, annealing and reverse proton exchange steps. These values are set to match the experimental process conditions, which are proprietary.

Table 1: Parameters for RPE Model

Parameter	Value	Units	Basis
D_{0e}	7.77×10^8	$\mu m^2/hr$	Lit[4]
Q	87.7	kJ/mol	Lit[4]
D_0	2.65×10^{11}	$\mu m^2/hr$	Lit[5]
T_0	1.67×10^4	K	Lit[5]
C_0	0.50	mol/m^3	Fit
α	0.127	m^3/mol	Lit[5]
Waveguide Width, W	5-9	μm	Exp

Exp = experimentally controlled parameter
Lit = value from literature
Fit = adjusted to fit experimental data

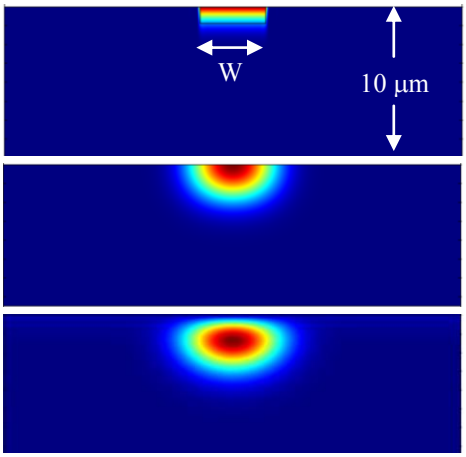

Figure 2. Impurity distribution (a) before annealing, (b) after annealing, (c) after reverse proton exchange

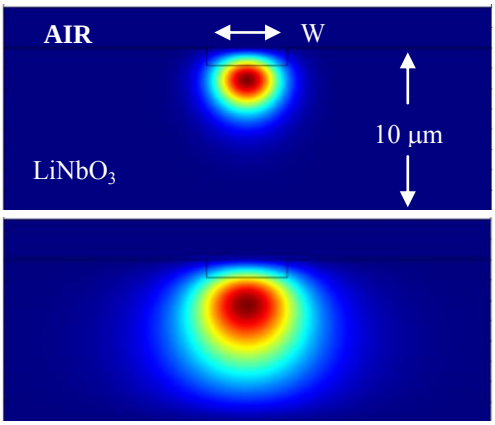

Figure 3. Fundamental optical mode field (E_y) at 986 nm (top) and 1972 nm

The effective indices of the modes were used to calculate the poling period from equation (3). The integrations of equation (8) were carried out within COMSOL by defining an integration coupling variable.

4. Results

4.1 Data Fitting

There are a number of parameters in the model that could be adjusted to fit the data, but to avoid over-fitting only one was adjusted: the fixed dopant concentration at the $LiNbO_3$ surface, C_0. A linear relationship between the index change and dopant concentration was assumed:

$$\Delta n = \alpha C \qquad (11)$$

Since in a linear model only the product of α and C_0 is significant, α was held fixed at a value of 0.127.

Several devices with different poling periods in the range of 15 to 19 μm were fabricated, and the second harmonic generation spectrum of each was measured. These devices produced a SHG peak with λ_1 in the 1.5 – 1.6 μm telecommunications band. C_0 was adjusted to fit the data for the SHG peak wavelength vs. poling period. The same model was then applied without modification to devices with Π = 25 to 30 μm, which produced a SHG peak at λ_1 = 1.8 to 2.1 μm. The results are shown in Figure 4. Given the peak wavelength, the model predicts the correct poling period within 0.5 micron.

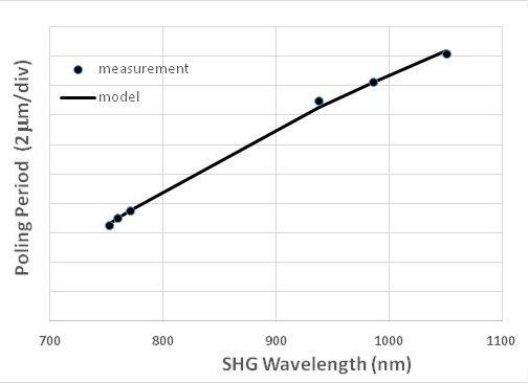

Figure 4. Calculated (line) and measured (markers) poling period vs. SHG peak wavelength

4.2 Input / Output Coupling Efficiency

The coupling efficiency vs. vertical offset (distance from the center of the fiber mode to the $LiNbO_3$ surface) was calculated from equation (8) for a 9 μm mode-field diameter fiber at several wavelengths. As shown in Figure 5, a minimum coupling loss of approximately 0.2 dB is predicted. The coupling is optimized in the 1.55 μm wavelength region.

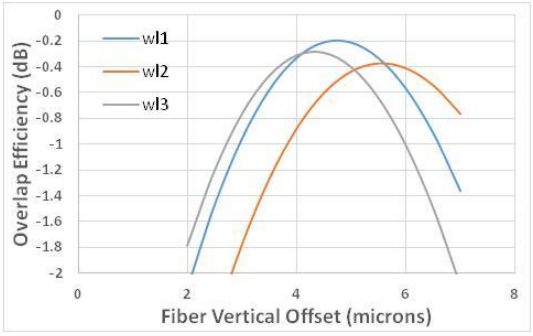

Figure 5. Calculated coupling efficiency from a 9 μm MFD single-mode fiber at several wavelengths vs. vertical offset.

4.3 Modal Effects and Conversion Efficiency

The previous discussion assumed single-mode operation, but in reality the waveguide is multi-moded at λ_1. The SHG spectrum contains multiple peaks corresponding to conversion of the input mode to various output modes. The relative amplitudes of the peaks depend on the overlap integrals calculated by equation (4) for each mode.

Figure 6 shows the measured SHG spectrum for a 1.0 cm-long RPE PPLN device, measured using a NKT Photonics supercontinuum (SC) source and a CCD spectrometer. The peak at 986 nm is due to conversion to the fundamental mode, and the peak at 909 nm is due to conversion to a higher-order mode. The corresponding computed mode field for the higher-order mode, which is a TM01-like mode, is shown in Figure 7.

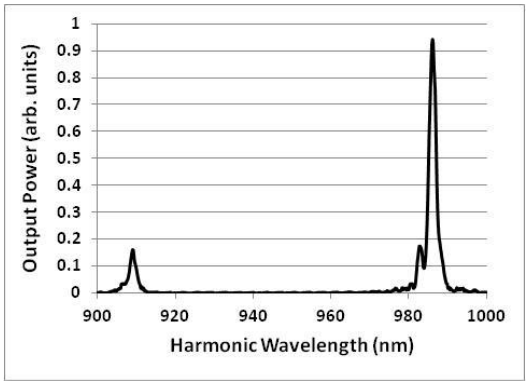

Figure 6. Measured SHG spectrum for RPE PPLN device

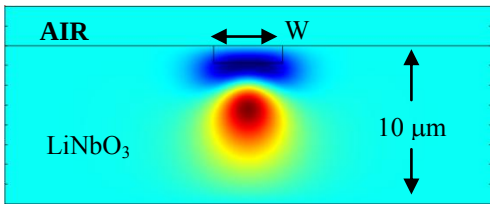

Figure 7. Computed higher-order (TM01-like) mode field (E_y) at 909 nm

Since equation (4) involves multiple modes, the integral cannot be carried out within Comsol 4.2 easily. Instead the mode profiles were exported from Comsol and post-processed in Scilab. To avoid difficulties associated with a non-uniform mesh, x- and y-cut lines through the peak of the mode field were exported, and the mode was reconstructed by assuming separability, that is E(x,y) = f(x)g(y). The calculated conversion efficiency values are given in Table 2.

Experimentally, the fiber-to-fiber SHG conversion efficiency for generation of the fundamental mode at 986 nm was estimated as approximately 40 %/W. However this is an upper limit, assuming that the phase matching bandwidth is equal to its theoretical value. (Assuming a wider bandwidth leads to a lower efficiency value.) Taking the ratio of the peak amplitudes in the SHG spectrum as a rough measure of the relative efficiency gives an upper limit of 7 %/W for the peak at 909 nm. Due to the uncertainty in the measurements, we can only say at this point that the model's predictions of conversion efficiency are roughly within a factor of two of the experimental values.

Table 2: Conversion Efficiency: Model vs. Measurement

λ_3 (nm) / Mode	η_{calc} %/Wcm^2	η_{exp} %/Wcm^2
986 TM00	18	<40
909 TM01	5.3	<7

5. Remaining Discrepancies and Future Work

Our current model allows prediction of the QPM period for SHG within 0.5 μm for input wavelengths between 1.5 and 2.0 μm. Conversely, this translates to an uncertainty of up to 10 nm in the peak wavelength for a given poling period. By contrast, the Stanford group [6] has reported the ability to predict the SHG peak wavelength within 2 nm consistently. However they have acknowledged that their model has been fit using data from a particular process and is much less accurate under different process conditions.

There are some additional features of the Stanford model that we may incorporate into ours, including nonlinear diffusion (concentration dependent diffusion coefficient), nonlinear dependence of Δn on concentration, and the presence of a "dead layer" near the surface in which the nonlinear optical coefficient is reduced. So far none of these extensions of the model have improved the agreement with experiment, but we plan to revisit them in the context of a systematic, multi-parameter optimization approach.

6. Conclusions

Comsol Multiphysics has been used to create a multi-step diffusion model, in conjunction with optical mode computations, for designing reverse proton exchanged waveguides in periodically poled lithium niobate for optical frequency conversion. After adjustment of a single fitting parameter, the model is able to predict the correct period for quasi-phase matching within 0.5 μm over the fundamental wavelength range of 1.5 to 2.0 μm. Efficiency calculations based on the computed modes have been carried out, but more precise measurements are needed to determine the accuracy of the calculations.

Further work will explore ways to improve the agreement between the model and measurements by incorporating nonlinear effects such as concentration-dependent diffusion, a quadratic concentration-refractive index relation, and the presence of a surface dead layer. The use of more formal parameter optimization schemes will also be studied.

7. References

1. A.P. VanDevender and P.G. Kwiat, "Quantum transduction via frequency upconversion," *J. Opt. Soc. Am. B* **24**, 295-9 (2007)
2. A. Martin, A. Issautier, H. Herrmann, W. Sohler, D.B. Ostrowsky, O. Alibart and S. Tanzilli, "A polarization entangled photon-pair source based on a type-II PPLN waveguide emitting at a telecom wavelength," *New J. Phys.* **12**, 103005 (2010)
3. P.E. Powers, *Fundamentals of Nonlinear Optics*, Chapters 4 - 7. CRC Press, Boca Raton (2011)
4. A. Loni, *An Experimental Study of Proton-Exchanged Lithium Niobate Optical Waveguides*, pp. 31-3. Ph.D. Thesis, University of Glasgow (1987)
5. M.M. Howerton, W.K. Burns, P.R. Skeath and A.S. Greenblatt, "Dependence of refraction index on hydrogen concentration in proton exchanged $LiNbO_3$," *IEEE J. Quantum Electron.* **27**, 593-601 (1991)
6. R.V. Roussev, *Optical Frequency Mixers in Periodically Poled Lithium Niobate: Materials, Modeling and Characterization*, pp. 16-53. Ph.D. Dissertation, Stanford University (2006) and references therein

8. Acknowledgements

We would like to thank NKT Photonics for the loan of a SuperK supercontinuum light source.